α-cluster microscopic study of ^{12}C + ^{12}C fusion toward the zero energy limit

T. Depastas [1,*] S. T. Sun,[2] H. Zheng [2] and A. Bonasera [1,3]

[1]*Cyclotron Institute, Texas A&M University, College Station, Texas 77843, USA*
[2]*School of Physics and Information Technology, Shaanxi Normal University, Xi'an 710119, China*
[3]*Laboratori Nazionali del Sud, INFN, Catania 95123, Italy*

The carbon burning process is a fundamental step of stellar evolution and governs the synthesis of chemical elements important for the formation of life. In this work, we utilize the microscopic hybrid α-cluster (HαC) model and an analytical approach, both in the framework of the imaginary time method (ITM), to study the carbon fusion reaction towards zero energy. We obtain the values of the cross sections and astrophysical factors and we correlate our results to collective motion. We also include a calculation for the 2^+ carbon fusion and discuss a possible experimental investigation. Our results confirm direct experimental and theoretical results close to the barrier, while suggesting possible 2^+ mixtures in the indirect experimental data. Our study offers an accurate view of the burning process in the somewhat unexplored low energy region.

I. INTRODUCTION

The carbon burning process (^{12}C + ^{12}C) is a key step in the evolution of massive stars and is the central theme of several recent studies. From a chemical perspective, this reaction plays a central role in the natural synthesis and abundances of the low mass elements of carbon, magnesium, oxygen, and sodium, all of them important for the formation of life. From the astrophysical point of view, this fusion is dominant in heavier stars with masses $\approx 8M_\odot$ and temperatures greater than 50 keV [1,2], as well as in x-ray bursts from accreting neutron stars [3,4]. The investigation of the cross sections and thus, reaction rates are important in our efforts to understand these phenomena. More specifically, the stellar reaction rates peak around the so-called Gamow energy [5], which for this case is below the Coulomb barrier, in the region of 1–2 MeV.

From the perspective of nuclear physics, carbon burning has already been investigated from the late 1960s [6]. Since then, several studies, both theoretical [7,8] and experimental [9–12], have been conducted for energies greater than $\approx$ 2.5 MeV. In this region, the theoretical results are more or less in agreement with the experimental data and show interesting collective characteristics [13].

The direct study of carbon fusion near the Gamow energy is experimentally challenging, as the cross section is an exponentially decreasing function of energy. Recent efforts by Tumino *et al.* [14], though, changed the situation. In their work, they studied the low energy fusion with the indirect Trojan horse method (THM) and were able to reach energies below 1 MeV [14]. This has opened the way for thorough investigations of the resonant structures that occur in this region

[7,15–17] and interesting discussions regarding the analysis of the relevant experimental data [10].

In this work, we aim to contribute to the study of the carbon fusion reaction, from a theoretical perspective, close to the region of zero energy. To achieve this, we employ microscopic and analytical models coupled with the imaginary time method (ITM) [7]. This has already been used successfully for fusion [7,13], fission [18], and multifragmentation reactions [19].

II. THEORETICAL FRAMEWORK

The hybrid α-cluster (HαC) model is a molecular dynamics approach, where the α particles are the fundamental degrees of freedom. The model Hamiltonian contains a potential energy with the following form [20]:

$$V = V_B + V_C. \tag{1}$$

The V_B term is the $A = 4$ Bass potential [21] that describes the nuclear interaction between the α particles, and V_C is the Coulomb potential, in the monopole-monopole approximation. To simulate the increase of the Fermi energy when the α particles are overlapping (due to the Pauli and Heisenberg correlations of their internal neutrons and protons), an extra kinetic energy term is added to the effective potential. This term has the form [20]

$$E_F = 4x_F \bar{\epsilon}_F \rho^{2/3}, \tag{2}$$

where $\bar{\epsilon}_F = 21$ MeV is the average kinetic energy due to internal Fermi motion and $x_F \approx 0.65$ is taken from reference [22]. This parameter is fixed for the α particles and takes into account both the Heisenberg and Pauli principles. The density of the α particles is defined as $\rho = 2e^{-\beta(r/r_\alpha)^2}$, with $\beta = 1.22$, $r_\alpha = r_0 4^{1/3}$, and $r_0 = 1.15$ fm [20]. The β parameter has been fitted to the ground state (g.s.) of ^{12}C, while the error of the

model binding energies for many α-cluster nuclei is $\approx 2\%$ [20]. The time evolution of the system is given by Hamiltonian equations of motion,

$$\frac{d\boldsymbol{p}_i}{dt} = \boldsymbol{F}_i = -\nabla_{\boldsymbol{r}_i}(V + E_F), \tag{3}$$

$$\frac{d\boldsymbol{r}_i}{dt} = \frac{\boldsymbol{p}_i}{m}, \tag{4}$$

where $\boldsymbol{F}_i$ is the total force that acts upon the particle i.

The ground state coordinates, i.e., $\boldsymbol{r}_i(t=0)$, are obtained via the solution of the equations of motion with a friction parameter. The ground state energies are reproduced well in the model for a wide range of $N = Z$ nuclei, with discrepancy of $\approx 2\%$ [20]. After the aforementioned "initialization" stage, the positions are randomly rotated and then are used as the initial conditions of Eqs. (3) and (4). The initial momenta are taken as zero. Each different set of random initial conditions is termed as a "random event." Our results come from an average of a few hundred random events.

The HαC model has already been used to study ^{12}C + ^{12}C fusion above the Coulomb barrier [20]. Microscopically, for the reaction $a + b \to c$ we consider the relative momentum P and position R of the system as

$$P = \mu_A(P_a - P_b), \tag{5}$$

$$R = R_a - R_b, \tag{6}$$

where $P_{a/b} = \frac{1}{A_{a/b}} \sum_{i \in a/b} P_{iz}$, $R_{a/b} = \frac{1}{A_{a/b}} \sum_{i \in a/b} R_{iz}$ are the collective degrees of freedom of the system in the reaction axis, $\mu_A = \frac{A_a A_b}{A_a + A_b}$ is the reduced mass number, while $A_{a/b}$ is the number of α particles located in the $R_z > 0$ or $R_z < 0$ plane respectively, with z being the reaction axis. The calculations start in real time until the system reaches the classical turning point [7]. In order to extend the use of the model into sub-barrier energies, we employ the Feynman path integral imaginary time method (ITM), first introduced in Ref. [7] for mean-field calculations. When the system reaches the outer classical turning point, we enter the imaginary time $t = i\tau$ and the collective momentum becomes $P = -i\Pi$. The equations of motion below the barrier result in a change of the sign to the forces, i.e., $F = -d\Pi/d\tau$. The equations of motion [Eqs. (3) and (4)] of the particle i in the nucleus a/b below the barrier are rewritten as

$$\frac{d\boldsymbol{p}_{i \in a/b}}{dt} = \boldsymbol{F}_i - \frac{F_{a/b}}{A_{a/b}}\hat{z}, \tag{7}$$

where $\frac{F_{a/b}}{A_{a/b}} = \frac{1}{A_{a/b}} \sum_{i \in a/b} F_{iz}$ is the collective force per particle. This ansatz simulates the sign inversion of only the collective part of the total force F_i that is exerted upon the particle i during imaginary times. In the analysis of fusion, the collective force comes from the Coulomb and Bass interactions, while the E_F interaction does not contribute, since it corresponds to the internal Fermi motion of the nuclei.

The probability of fusion in the different l channels is calculated from the relation [7]

$$T_l(E_{\text{C.M.}}) = \begin{cases} (1 + e^{2A/\hbar})^{-1}, & l = 0, \\ T_0\left(E_{\text{C.M.}} - \frac{l(l+1)\hbar^2}{2\mu R_N^2}\right), & l > 0, \end{cases} \tag{8}$$

where $A = \int \Pi\, dR$ is the action of the collective motion during imaginary time evolution. The probabilities for higher angular momenta are approximated by a $\frac{l(l+1)\hbar^2}{2\mu R_N^2}$ shift in the energy [7]. This term represents the semiclassical centrifugal potential, and $R_N = R_a + R_b = 2r_g 12^{1/3}$ and $r_g = 1.4$ fm, which takes into account the range of the nuclear force that extends farther than the nuclear density. With the use of the probabilities [Eq. (8)], the cross section for the center-of-mass energy $E_{\text{C.M.}}$ is obtained via the formula

$$\sigma(E_{\text{C.M.}}) = \frac{\pi\hbar^2}{\mu E_{\text{C.M.}}} \sum_{l=0}^{\infty} (2l+1)T_l(E_{\text{C.M.}})\delta_{l,\text{even}}, \tag{9}$$

where l can only take even values, since the two reacting ^{12}C are identical bosons and thus, parity must be positive. We define the astrophysical $S(E_{\text{C.M.}})$ factor and its modified version $S^*(E_{\text{C.M.}})$ as [6]

$$S^*(E_{\text{C.M.}}) = E_{\text{C.M.}}\sigma(E_{\text{C.M.}})e^{\xi/\sqrt{E_{\text{C.M.}}} + 0.46E_{\text{C.M.}}}$$

$$= S(E_{\text{C.M.}})e^{0.46E_{\text{C.M.}}}, \tag{10}$$

where $\xi = Z_a Z_b \pi e^2 \sqrt{2\mu}/\hbar = 87.23$ MeV$^{1/2}$.

We also extend the analytical approach of Ref. [23], with the use of the ITM. Specifically, by considering a square well nuclear potential with radius R_N, the action below the Coulomb barrier is written as

$$\begin{aligned} A &= \int \Pi\, dR = \sqrt{2\mu E_{\text{C.M.}}} \int_{R_N}^{R_c} dR \sqrt{\frac{Z_a Z_b e^2}{R E_{\text{C.M.}}} - 1} \\ &= \sqrt{2\mu E_{\text{C.M.}}} \int_0^{R_c} dR \sqrt{\frac{Z_a Z_b e^2}{R E_{\text{C.M.}}} - 1} \\ &\quad - \sqrt{2\mu E_{\text{C.M.}}} \int_0^{R_N} dR \sqrt{\frac{Z_a Z_b e^2}{R E_{\text{C.M.}}} - 1} \\ &\equiv A_G - A_N, \end{aligned} \tag{11}$$

where A_G is the action in the Gamow limit (i.e., only Coulomb) and A_N is the nuclear contribution to the action. The values of A_G [23] and A are respectively

$$A_G = \frac{\hbar\xi}{2E_{\text{C.M.}}} = Z_a Z_b \pi e^2 \sqrt{\frac{\mu}{2E_{\text{C.M.}}}}, \tag{12}$$

$$\begin{aligned} A &= Z_a Z_b e^2 \sqrt{\frac{2\mu}{E_{\text{C.M.}}}} \tan^{-1}\left(\sqrt{\frac{Z_a Z_b e^2}{E_{\text{C.M.}} R_N} - 1}\right) \\ &\quad - R_N \sqrt{2\mu\left(\frac{Z_a Z_b e^2}{R_N} - E_{\text{C.M.}}\right)}. \end{aligned} \tag{13}$$

In order to take into account the finite sizes of the nuclei, we introduce a screening to the Coulomb potential, of the form

$$V_{sc} = \frac{Z_a Z_b e^2}{R}(1 - e^{-\lambda R}). \tag{14}$$

The value of screening parameter λ is estimated via the difference of the compound and reactant nuclei Coulomb

contributions. From the semiempirical mass formula in the limit of small distances,

$$V_{sc} \approx \frac{Z_a Z_b e^2}{R}(1 - 1 + \lambda R) = \lambda Z_a Z_b e^2$$

$$= |E_C(^{A_c}c) - E_C(^{A_a}a) - E_C(^{A_b}b)|, \qquad (15)$$

or equivalently

$$\lambda = \frac{a_c}{Z_a Z_b e^2} \left| \frac{(Z_a + Z_b)(Z_a + Z_b - 1)}{(A_a + A_b)^{1/3}} \right.$$

$$\left. - \frac{Z_a(Z_a - 1)}{A_a^{1/3}} - \frac{Z_b(Z_b - 1)}{A_b^{1/3}} \right|, \qquad (16)$$

with $a_c = 0.75$ MeV. For $Z_a = Z_b = Z = 6$ and $A_a = A_b = A = 12$, the screening parameter takes the value

$$\lambda = \frac{2a_c}{Z A^{1/3} e^2} |(2^{2/3} - 1)Z + 1 - 2^{-1/3}| = \frac{1}{3.535 \text{ fm}}. \quad (17)$$

The actions that correspond to the Coulomb (A_{SC}) and Nuclear ($A_{N,SC}$), as well as the total contributions (A_{eff}), are given by the following integrals:

$$A_{\text{eff}} = \sqrt{2\mu E_{\text{C.M.}}} \int_0^{R_c} dR \sqrt{\frac{Z_a Z_b e^2}{R E_{\text{C.M.}}}(1 - e^{-\lambda R}) - 1}$$

$$- \sqrt{2\mu E_{\text{C.M.}}} \int_0^{R_N} dR \sqrt{\frac{Z_a Z_b e^2}{R E_{\text{C.M.}}}(1 - e^{-\lambda R}) - 1}$$

$$\equiv A_{SC} - A_{N,SC}. \qquad (18)$$

These integrals are solved numerically. The value of the Gamow energy in different approximation schemes is given by the dominant contribution to the reaction rate integral [Ref. [5], Eq. (1)]

$$\langle \sigma v \rangle = \sqrt{\frac{8}{\mu\pi(kT)^3}} \int_0^\infty S(E) e^{-\frac{\xi}{\sqrt{E}} - \frac{E}{kT}} dE. \qquad (19)$$

The dominant contribution is then taken from the maximization of the integrand:

$$\frac{\xi E^{-3/2}}{2} S(E) + \frac{dS}{dE} = \frac{S(E)}{kT}, \qquad (20)$$

where the usual temperature in stellar scenarios is $kT \approx 50$ keV, for carbon stars [1]. In the pure Coulomb limit [i.e., Eq. (12)] the Gamow energy is $E_G = 1.682$ MeV; considering the nuclear contribution [i.e., Eq. (13)] it is $E_{G+N} = 1.634$ MeV. The screened Coulomb potential with the nuclear contribution [i.e., Eq. (18)] gives $E_{SC} = 1.711$ MeV and $E_{SC+N} = 1.643$ MeV. The small differences among the various approximations indicate that most of the action contribution comes from Coulomb force at large distances. Thus it is important that our simulations are stable for long times, which correspond to large distances and very small beam energies (in the keV region).

III. RESULTS AND DISCUSSION

Within the HαC model, at a given beam energy, the nuclei move towards each other until they stop at the outer turning point due to the Coulomb force. We switch to imaginary time, by inverting the collective forces [Eq. (7)], until they stop at the inner turning point. A typical example for $E_{\text{C.M.}} = 3.5$ MeV is shown in Fig. 1. The total energy of the system during the imaginary time evolution is not conserved due to the work done by the collective forces. The final energy (i.e., in real time) corresponds to the ^{24}Mg ground state and the reaction Q value, experimentally measured as $Q_{\text{exp}} = 13.933$ MeV, a value reproduced in the model within a few keV; see Fig. 2. In contrast, the energy is conserved during real time evolution, as expected. We present calculations of the action for several energies in the aforementioned range with the HαC model. We fit this, opportunely normalized by A_G [Eq. (12)], as an exponential function of the energy [16]. The calculated points and the numerical fit are shown in Fig. 3. From this, we extract the value of the effective Coulomb barrier (which comes from the interplay of Coulomb force with the nuclear potential) at 5.89 MeV. This is defined as the energy where the system fuses without entering into imaginary time, i.e., $A = 0$, and its value is close to the one reported in Ref. [16]. The action is a simpler function and thus could be used instead of the S and S^* factors to report the data as well [16]. Furthermore, we obtain the cross sections and the astrophysical factors for several energies from 0 to 7 MeV. We note that, in the energy range specified, there are no contributions for $l > 6$. Our results for different l values obtained with the HαC model and the corresponding results from the analytical approach [$l = 0$, with free and screened Coulomb force, Eqs. (13) and (18)] are shown in Fig. 4 (top). The analytical approach gives results that are generally similar to the HαC model, except for some oscillations of collective nature. Additionally, we see that the $l = 0$ wave is dominant up to 4.5 MeV and the $l = 2$ wave dominates up to 6.5 MeV. At higher energies, we see the increase of $l = 4$ contributions. The $l = 6$ result is off the scale of Fig. 4 (top), since it only contributes up to 0.08% of the total S^* factor.

In the bottom panel of Fig. 4, we plot the S^* factors versus energy from several experimental [9,11,12,14,24,25] and theoretical [7,26] approaches. The results from this work (HαC model) are represented by the red curve, for all l values. Similarly to the results obtained with the neck model (NM) [15,27], time dependent Hartree-Fock [28], and the Vlasov [7] approaches (dark green, Fig. 4), our calculations yield S^* as a smooth function of energy, except for some small oscillations, within the range $\approx 10^{15}$–10^{17} MeV b. The general trend of the experimental data in the $E > 2.5$ MeV region is followed, while the discrepancies from the Tumino data [14] are explained by the absence of the ^{24}Mg resonant levels [15,27] in the semiclassical HαC model. We note that our S^* results depend somewhat on the choice of the nuclear equation of state (EoS), i.e., the values of β and r_0 in Eq. (2). For the purpose of the present study, we used the EoS of Ref. [20]. Interestingly, with our approach no hindrance effects are observed [8], as also seen in the macroscopic study of Ref. [29]. The antisymmetrized molecular dynamics (AMD) approach [26] also gives a smooth function of S^*, although with larger oscillations and generally lower values (crosses in Fig. 4 bottom panel). This might be due to an overestimation of binding energies with the AMD model, at variance to other
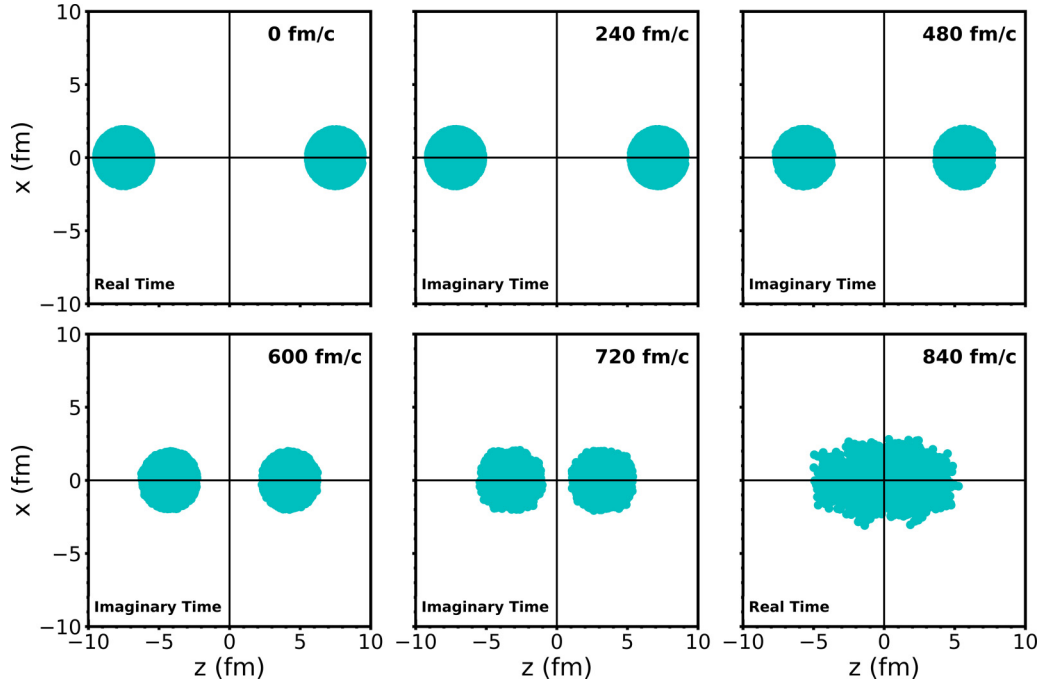
FIG. 1. Evolution of the ^{12}C $+$ ^{12}C fusion in the xz plane with $E_{\text{C.M.}} = 3.5$ MeV. The cyan points are the densities of the α particles from 300 event calculations with the HαC model, while the reaction axis is defined to be the z axis.

dynamical approaches like the constrained molecular dynamics (CoMD) model [30,31].

The orange curve in Fig. 4, bottom panel, represents the results of the ^{12}C(g.s.) $+$ ^{12}C(4.44 MeV, 2^+) reaction, with the HαC model. To prepare the excited state, we consider a linear configuration, with the quantized-rotation scheme given by Eq. (5) of Ref. [20], while the initial $\alpha - \alpha$ distances are fitted to the binding energy. We observe that the S^* factors are enhanced when compared to the g.s. reaction, while similar oscillations are also present. Such situations may occur

in stars despite being highly improbable for carbon-burning stars. However, they are important for α-burning stars where ^{12}C is formed through triple α reactions in an excited state and possibly reacts with lighter particles (p, n, or α). These effects can influence the carbon decay width into 3α or via γ emission [32,33].

The goal of the present excited-state calculations is to stimulate some experimental investigations using the THM. For instance in Ref. [14] the reaction ^{14}N $+$ ^{12}C was used, with the deuteron in ^{14}N being the spectator. In these
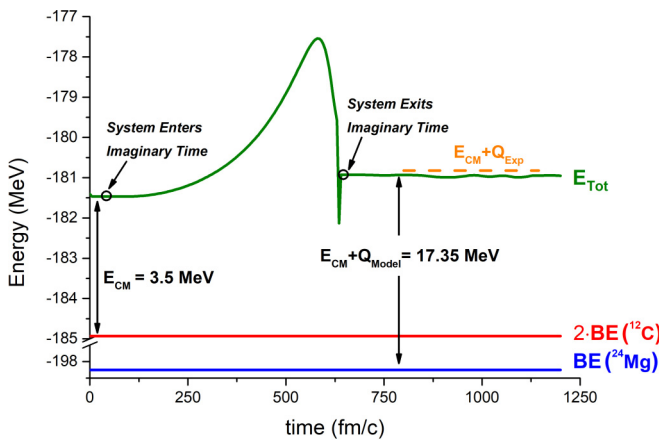

FIG. 2. Evolution of the total energy (green line) of the system during fusion with $E_{\text{C.M.}} = 3.5$ MeV, as calculated with the HαC model. The blue and red lines correspond to the ground state energies of ^{24}Mg and ^{12}C $+$ ^{12}C, respectively. The dashed orange line, corresponds to the final energy with the experimental $Q = 13.933$ MeV value.
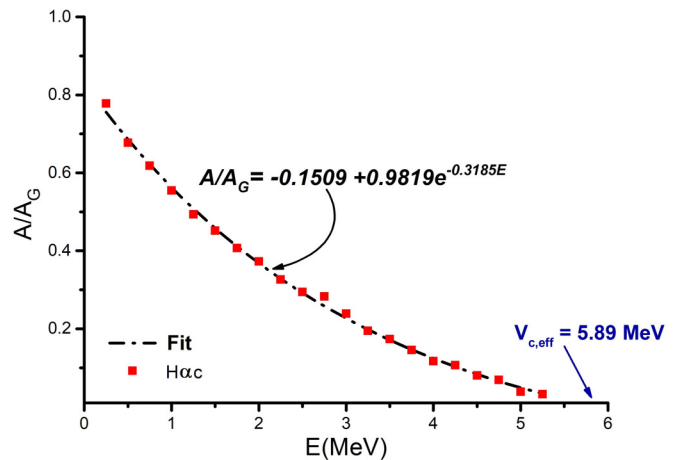

FIG. 3. The $l = 0$ channel action A normalized by the same quantity in the Gamow limit [A_G, Eq. (12)] as function of energy (red points), as obtained via the HαC model. The dashed line corresponds to an exponential fit. We indicate the value of the effective Coulomb barrier at 5.89 MeV.

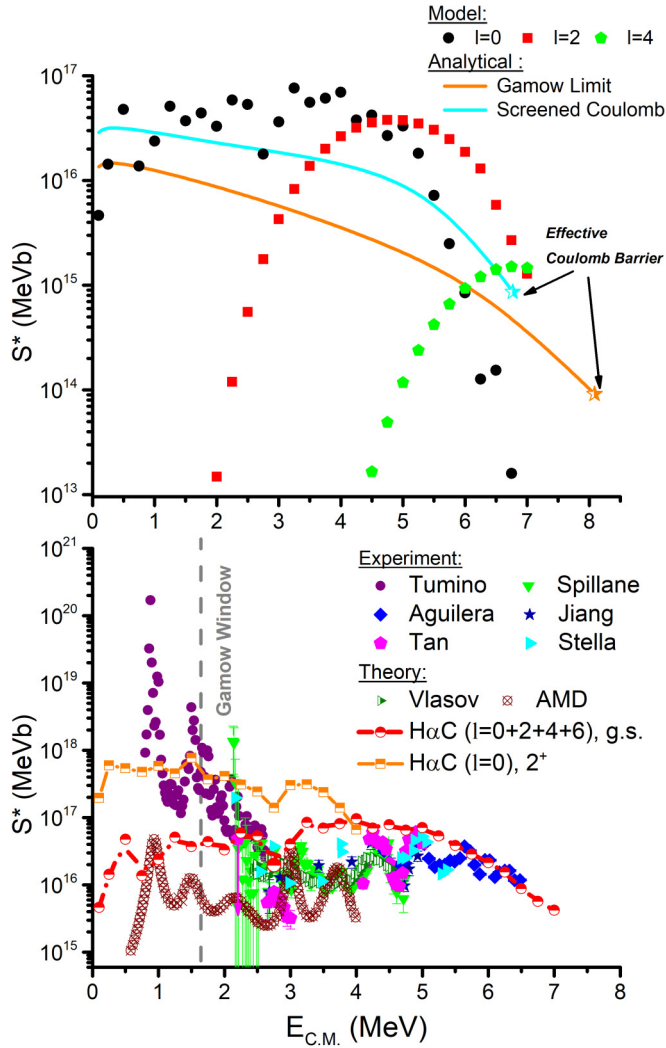FIG. 4. Top panel: The S^* factors as a function of energy for different l values (points) obtained via the HαC model and via the analytical approach with free and screened Coulomb (lines), according to the key. Bottom panel: The S^* factors as a function of energy from several experimental [9,11,12,14,24,25] and theoretical [7,26] data sets. This work corresponds to the red curve for all l values (g.s.) and the orange curve (4.44 MeV, 2^+), as obtained with the HαC model. The pink arrow corresponds to the lowest energy direct measurement [25] and represents an upper limit.

FIG. 5. The reaction rate $\langle \sigma v \rangle$ scaled by the corresponding rate $\langle \sigma v \rangle_0$ obtained via a constant factor $S_0 = 10^{16}$ MeV b, as a function of temperature. The dashed lines denote regions of astrophysical interest [14].

Eq. (19), we calculate the value of $\langle \sigma v \rangle$ as a fraction of the corresponding quantity ($\langle \sigma v \rangle_0$) calculated via the constant $S_0 = 10^{16}$ MeV b. Our results as a function of temperature, for both the ground state and 2^+ fusion, are presented in Fig. 5. We also indicate several important astrophysical regions. The higher reaction rates have serious implications for the natural relative element abundances in stars. In Fig. 6 we present our attempt to correlate the oscillation of S^* with resonances
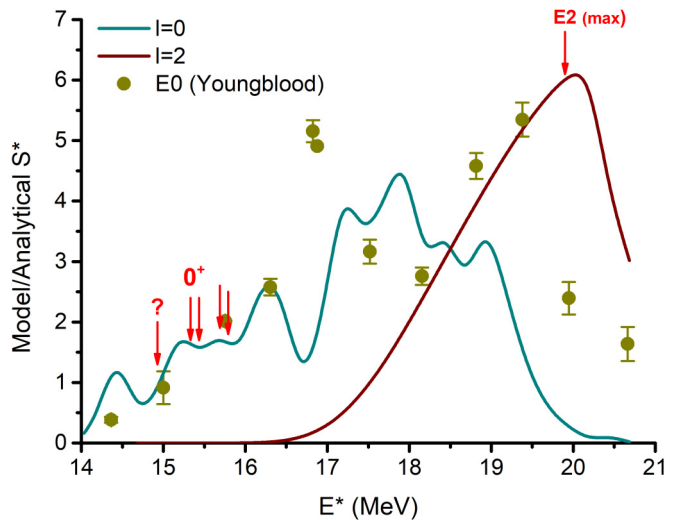
FIG. 6. The ratio of S^* values calculated via the HαC model divided by the corresponding analytical values [Eqs. (10) and (18)], for different l values (solid lines) as a function of $E^* = E_{\text{C.M.}} + Q$. The points represent the experimental isoscalar monopole ($E0$) spectrum of ^{24}Mg [37]. We indicate the energy of isoscalar ^{24}Mg quadrupole ($E2$) peak [37] with a red arrow. We also include the position of the 0^+ experimental levels of ^{24}Mg with red arrows [36]. The experimental points are normalized to the intersection with the $l = 0$ curve at 16.4 MeV.

reactions it may happen that the deuteron carries some angular momentum, leaving the ^{12}C in the 2^+, 4.44 MeV excited level. The authors of Ref. [14] were aware of this possibility and they investigated the angular distribution of fusion events at the lowest C.M. energies [34] and found those events to be compatible with $l = 0$ angular momenta. Nevertheless, our result suggests otherwise. Similar indications can be inferred also from coupled-channels calculations [35]. There, several excited states have been taken into account, with the justification that the carbon atoms could be initially in an excited state, due to Coulomb excitation. The enhancement of the astrophysical factor of 2^+ fusion by a factor of ≈ 10–100 results in a ≈ 10–100 times increased reaction rates. Using
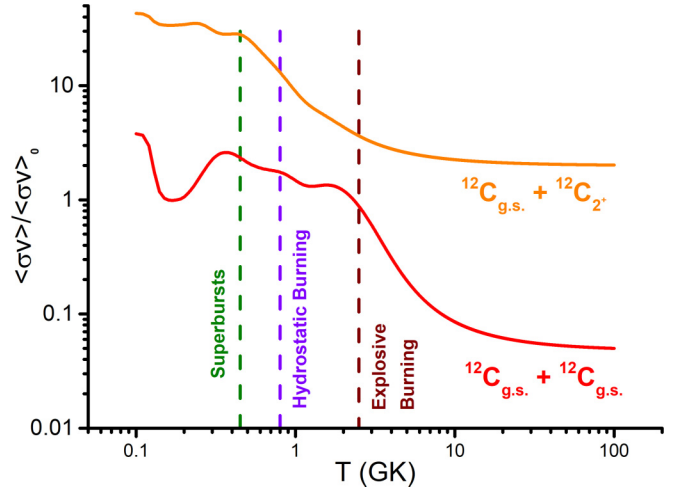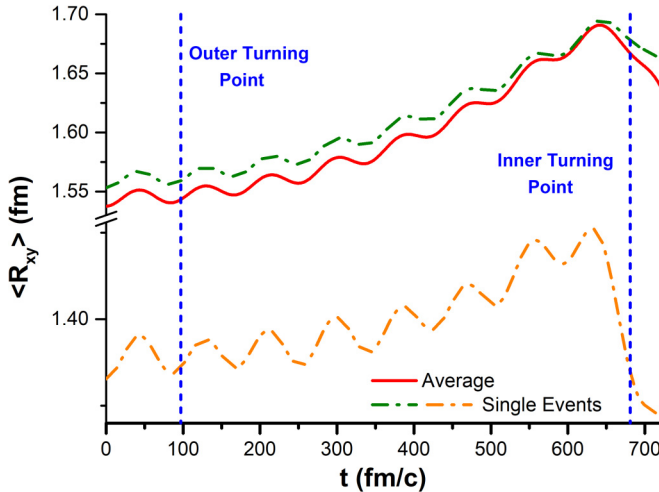
FIG. 7. The transverse mean radius $\langle R_{xy} \rangle = \sqrt{\langle x^2 + y^2 \rangle}$ of the $E_{\text{C.M.}} = 3.5$ MeV reaction, for two single events (dashed curves) and as an average of 300 events (solid curve). The vertical lines show the average turning points of the carbon-carbon system, as calculated via the HαC model.

of ^{24}Mg. The differences in S^* between the HαC model and the analytical formulas mostly come from the collective motions of the constituent α particles, that naturally arise in our dynamical approach. In that sense, the ratio of S^* values obtained via the HαC model divided by its counterpart from the analytical formulas [Eqs. (10) and (18)] represents the collective contributions of the compound ^{24}Mg nucleus to the astrophysical factor. The polarity of the giant resonant motion comes from the l value of the reaction. The spectra for $l = 0$ and $l = 2$ as functions of the excitation energy, i.e., $E^* = E_{\text{C.M.}} + Q$, are shown by the solid lines in Fig. 6. The arrows are the 0^+ excited levels of ^{24}Mg [36] (the question mark shows a level with uncertainty to its spin-parity). As we have already mentioned, these levels do not appear in our semiclassical model. The points correspond to a part of the isoscalar monopole ($E0$) spectrum of ^{24}Mg [37], while the maximum of the isoscalar quadrupole (E2) response is also denoted with an arrow [37]. The $l = 0$ oscillations qualitatively show a trend similar to that of the $E0$ peaks, while the $l = 2$ peak represents quite accurately the maximum of the $E2$ spectrum. The $E0$ in the experimental data [37], might

not represent a monopole response, but a coupling of $K0$ of the quadrupole mode of magnesium [38]. The nature of the aforementioned collective oscillations can be understood in terms of the mean transverse radius, i.e., $\langle R_{xy} \rangle = \sqrt{\langle x^2 + y^2 \rangle}$, averaged over the α particle coordinates. In Fig. 7, we plot $\langle R_{xy} \rangle$ over time for the $E_{\text{C.M.}} = 3.5$ MeV reaction. The solid curve corresponds to the moment averaged over 300 events (in a manner similar to Fig. 1), while the dashed curves describe the moment for two single events and the vertical lines show the average turning points. The oscillations of these curves signify a transverse oscillation of the system during imaginary time, which gives rise to oscillations in action and in turn to the S^* factor.

IV. CONCLUSION

To conclude, we studied the ^{12}C + ^{12}C fusion at sub-barrier energies within the 0–7 MeV region. Our approach is based on a microscopic dynamical model with α degrees of freedom (HαC) and an analytical approach including the screening of the Coulomb potential. Both of these processes are performed in the framework of the imaginary time method (ITM). With both numerical and analytical approaches we obtain the values of $S^*(E)$. Our results agree with recent experimental data, apart from resonant peaks, while we confirm theoretical approaches performed via the Vlasov [7], AMD [26], and NM [15,27] methods. The evolution of the system during imaginary time shows some interesting physical characteristics, such as the involvement of isoscalar giant resonance modes, during the imaginary evolution. Predictions for fusion of ^{12}C nuclei in excited levels are also included and we suggest investigating this case with the THM. Finally, the coupling of the HαC model with the ITM opens the way for theoretical investigation of other $N = Z$ fusions involving both ground and excited nuclear states.

[1] C. E. Rolfs and W. S. Rodney, *Cauldrons in the Cosmos: Nuclear Astrophysics* (University of Chicago Press, Chicago, 1988).

[2] C. Iliadis, *Nuclear Physics of Stars* (Wiley, Weinheim, 2007).

[3] A. Cumming and L. Bildsten, Astrophys. J. **559**, L127 (2001).

[4] L. Keek, A. Heger, and J. J. M. in 't Zand, Astrophys. J. **752**, 150 (2012).

[5] S. Kimura and A. Bonasera, Phys. Rev. C **87**, 058801 (2013).

[6] J. Patterson, H. Winkler, and C. Zaidins, Astrophys. J. **157**, 367 (1969).

[7] A. Bonasera and V. Kondratyev, Phys. Lett. B **339**, 207 (1994).

[8] C. L. Jiang, K. E. Rehm, B. B. Back, and R. V. F. Janssens, Phys. Rev. C **75**, 015803 (2007).

[9] E. F. Aguilera *et al.*, Phys. Rev. C **73**, 064601 (2006).

[10] C. Beck, A. Mukhamedzhanov, and X. Tang, Eur. Phys. J. A **56**, 87 (2020).

[11] C. L. Jiang, D. Santiago-Gonzalez, S. Almaraz-Calderon, K. E. Rehm, B. B. Back, K. Auranen, M. L. Avila, A. D. Ayangeakaa, S. Bottoni, M. P. Carpenter, C. Dickerson, B. DiGiovine, J. P. Greene, C. R. Hoffman, R. V. F. Janssens, B. P. Kay, S. A. Kuvin, T. Lauritsen, R. C. Pardo, J. Sethi *et al.*, Phys. Rev. C **97**, 012801(R) (2018).

[12] T. Spillane *et al.*, Phys. Rev. Lett. **98**, 122501 (2007).

[13] V. N. Kondratyev, A. Bonasera, and A. Iwamoto, Phys. Rev. C **61**, 044613 (2000).

[14] A. Tumino *et al.*, Nature (London) **557**, 687 (2018).

[15] A. Bonasera and J. B. Natowitz, Phys. Rev. C **102**, 061602(R) (2020).

[16] A. Bonasera, EPJ Web Conf. **252**, 05001 (2021).

[17] P. Adsley *et al.*, Phys. Rev. Lett. **129**, 102701 (2022).

[18] A. Bonasera and A. Iwamoto, Phys. Rev. Lett. **78**, 187 (1997).

[19] T. Maruyama, A. Bonasera, and S. Chiba, Phys. Rev. C **63**, 057601 (2001).

[20] H. Zheng and A. Bonasera, Symmetry **13**, 1777 (2021).

[21] R. Bass, Phys. Rev. Lett. **39**, 265 (1977).

[22] A. Bonasera, F. Gulminelli, and J. Molitoris, Phys. Rep. **243**, 1 (1994).

[23] S. Kimura and A. Bonasera, Phys. Rev. C **76**, 031602(R) (2007).

[24] G. Fruet *et al.*, Phys. Rev. Lett. **124**, 192701 (2020).

[25] W. P. Tan *et al.*, Phys. Rev. Lett. **124**, 192702 (2020).

[26] Y. Taniguchi and M. Kimura, Phys. Lett. B **823**, 136790 (2021).

[27] A. Bonasera, G. Bertsch, and E. El-Sayed, Phys. Lett. B **141**, 9 (1984).

[28] A. Diaz-Torres and M. Wiescher, Phys. Rev. C **97**, 055802 (2018).

[29] K. Godbey, C. Simenel, and A. S. Umar, Phys. Rev. C **100**, 024619 (2019).

[30] M. Papa, T. Maruyama, and A. Bonasera, Phys. Rev. C **64**, 024612 (2001).

[31] G. Giuliani, H. Zheng, and A. Bonasera, Prog. Part. Nucl. Phys. **76**, 116 (2014).

[32] M. Beard, S. M. Austin, and R. Cyburt, Phys. Rev. Lett. **119**, 112701 (2017).

[33] J. Bishop *et al.*, Nat. Commun. **13**, 2151 (2022).

[34] A. Tumino (private communication).

[35] L. Gasques, L. Chamon, and G. Cessel, Eur. Phys. J. A **58**, 102 (2022).

[36] M. S. Shamsuzzoha Basunia and A. Chakraborty, Nucl. Data Sheets **186**, 3 (2022).

[37] D. H. Youngblood, Y.-W. Lui, X. F. Chen, and H. L. Clark, Phys. Rev. C **80**, 064318 (2009).

[38] A. Bahini, V. O. Nesterenko, I. T. Usman, P. von Neumann-Cosel, R. Neveling, J. Carter, J. Kvasil, A. Repko, P. Adsley, N. Botha, J. W. Brummer, L. M. Donaldson, S. Jongile, T. C. Khumalo, M. B. Latif, K. C. W. Li, P. Z. Mabika, P. T. Molema, C. S. Moodley, S. D. Olorunfunmi *et al.*, Phys. Rev. C **105**, 024311 (2022).